



PCCP

**Photoelectron spectroscopy and computational investigations of the electronic structures and noncovalent interactions of cyclodextrin-closo-dodecaborate anion complexes X-CD-B12X122– (X =  $\alpha$ ,  $\beta$ ,  $\gamma$ ; X = H, F)**

Journal:	<i>Physical Chemistry Chemical Physics</i>
Manuscript ID	CP-ART-02-2020-000700.R1
Article Type:	Paper
Date Submitted by the Author:	04-Mar-2020
Complete List of Authors:	Li, Zhipeng ; East China Normal University, State Key Laboratory of Precision Spectroscopy Jiang, Yanrong; East China Normal University, State Key Laboratory of Precision Spectroscopy Yuan, Qinqin; Pacific Northwest National Laboratory, Physical Sciences Division Warneke, Jonas; Universität Leipzig, Wilhelm-Ostwald-Institut für Physikalische und Theoretische Chemie Hu, Zhubin; East China Normal University, State Key Laboratory of Precision Spectroscopy Yang, Yan; East China Normal University, Precision Spectrometry Sun, Haitao; State Key Laboratory of Precision Spectroscopy, Department of Physics Sun, Zhenrong; East China Normal University, State Key Laboratory of Precision Spectroscopy Wang, Xue-Bin; Pacific Northwest National Laboratory, Physical Sciences Division

SCHOLARONE™  
Manuscripts

## ARTICLE

# Photoelectron spectroscopy and computational investigations of the electronic structures and noncovalent interactions of cyclodextrin-*closo*-dodecaborate anion complexes $\chi$ -CD·B<sub>12</sub>X<sub>12</sub><sup>2-</sup> ( $\chi$ = $\alpha$ , $\beta$ , $\gamma$ ; X = H, F)

Received 00th January 20xx,  
Accepted 00th January 20xx

DOI: 10.1039/x0xx00000x

Zhipeng Li,<sup>a,b,§,‡</sup> Yanrong Jiang,<sup>a,‡</sup> Qinqin Yuan,<sup>b,§</sup> Jonas Warneke,<sup>c</sup> Zhubin Hu,<sup>a</sup> Yan Yang,<sup>a</sup> Haitao Sun,<sup>\*a,d</sup> Zhenrong Sun<sup>\*a,d</sup> and Xue-Bin Wang<sup>\*b</sup>

We report a joint negative ion photoelectron spectroscopy (NIPES) and computational study on the electronic structures and noncovalent interactions of a series of cyclodextrin-*closo*-dodecaborate dianion complexes,  $\chi$ -CD·B<sub>12</sub>X<sub>12</sub><sup>2-</sup> ( $\chi$  =  $\alpha$ ,  $\beta$ ,  $\gamma$ ; X = H, F). The measured vertical / adiabatic detachment energies (VDEs / ADEs) are 1.15/0.93, 3.55/3.20, 3.90/3.60, and 3.85/3.60 eV for B<sub>12</sub>H<sub>12</sub><sup>2-</sup> and its  $\alpha$ -,  $\beta$ -,  $\gamma$ -CD complexes, respectively; while the corresponding values are 1.90/1.70, 4.00/3.60, 4.33/3.95, and 4.30/3.85 eV for the X = F case. These results show that the inclusion of B<sub>12</sub>X<sub>12</sub><sup>2-</sup> into the CD cavities greatly increase the electronic stability of the dianions. The effect of electronic stabilization for  $\beta$ -CD is roughly the same as for  $\gamma$ -CD, both being considerably stronger than that for  $\alpha$ -CD. Density functional theory (DFT) based geometry optimization reveals that B<sub>12</sub>X<sub>12</sub><sup>2-</sup> are inserted into CDs increasingly deeper from  $\alpha$ -CD to  $\gamma$ -CD. The calculated VDEs and ADEs agree with the experiments well, particularly, reproducing the electron binding energy (EBE) trends. The molecular orbital analyses indicate that the most loosely bound photodetached electrons origin from the guest B<sub>12</sub>X<sub>12</sub><sup>2-</sup> moieties. In addition to a shift of all signals to larger EBE, significant changes in the signal patterns are observed. At low EBE, this is due to the splitting of highly degenerate B<sub>12</sub>X<sub>12</sub><sup>2-</sup> orbitals, while at high EBE, photodetachment from CD oxygens contributes to the new bands. The guest B<sub>12</sub>X<sub>12</sub><sup>2-</sup> and host CD noncovalent, size-specific interaction based on the independent gradient model (IGM) and energy decomposition analysis (EDA), is dominated by electrostatic interactions. The analysis further unravels unambiguously the existence of dihydrogen bonding and how it affects the total energy that stabilizes the host-guest complexes of CDs·B<sub>12</sub>H<sub>12</sub><sup>2-</sup> compared to the general hydrogen bonding interaction in CDs·B<sub>12</sub>F<sub>12</sub><sup>2-</sup>. This work clearly exhibits strong influences on the electronic structures of dodecaborates upon clustering with CDs, with both size ( $\alpha$ -,  $\beta$ -,  $\gamma$ -) and molecular (X = H or F) specificities, thus providing critical molecular-level information on the cyclodextrin-*closo*-dodecaborate interactions of interest to medical applications, e.g. Boron neutron capture therapy.

## 1. Introduction

The *closo*-dodecaborate dianions possess icosahedral molecular symmetry with highly delocalized charge distribution, exceptional electronic, and thermodynamic stability.<sup>1-8</sup> Owing to these unique molecular properties, they have been widely tested, for examples, as electrolytes in lithium batteries<sup>9, 10</sup>, and building blocks of non-linear optics materials,<sup>11, 12</sup> with numerous applications, for examples, in

chemical synthesis, catalysis,<sup>6, 13-16</sup> and boron neutron capture therapy (BNCT)<sup>17-19</sup>. The electronic structures and electron loss process of a series of homogeneous *closo*-dodecaborate dianions B<sub>12</sub>X<sub>12</sub><sup>2-</sup> (X = H, F, Cl, Br, I, At) have been recently studied, confirming their electronic stability in the gas phase and further unravelling the critical role and tunability of substituent shell X<sub>12</sub> in determining their molecular properties.<sup>20, 21</sup> For the potential application of the B<sub>12</sub>X<sub>12</sub><sup>2-</sup> dianions in BNCT clinical treatments, the factors such as high stability, high boron content and low toxicity are important.<sup>2, 22</sup> Biological tests revealed that naked dodecaborate anions are difficult to penetrate through cell membranes, which significantly lowers the boron content within the targeted cancer cells.<sup>19, 22</sup>

One possible approach for effective delivery of dodecaborate dianions into cells is to bind them within the cavities of host molecules (to form host-guest inclusion complexes) which can mask their chemical signature and facilitate passing them through the cell walls. Cyclodextrins (CDs) (see Fig. S1 in ESI†) with lipophilic inner cavities and

<sup>a</sup> State Key Laboratory of Precision Spectroscopy, East China Normal University, Shanghai 200062, China

<sup>b</sup> Physical Sciences Division, Pacific Northwest National Laboratory, 902 Battelle Boulevard, P.O. Box 999, Richland, Washington 99352, USA

<sup>c</sup> Wilhelm-Ostwald-Institut für Physikalische und Theoretische Chemie, Universität Leipzig, 04103 Leipzig, Germany.

<sup>d</sup> Collaborative Innovation Center of Extreme Optics, Shanxi University, Taiyuan, Shanxi 030006, China

<sup>§</sup> Visiting students supported via PNNL alternate sponsored fellowship program  
<sup>‡</sup> Z. Li, and Y. Jiang contributed equally in this work.

\*Corresponding author: xuebin.wang@pnnl.gov (X.-B.W.);  
htsun@phy.ecnu.edu.cn (H.-T.S) and zrsun@phy.ecnu.edu.cn (Z.-R.S).

†Electronic Supplementary Information (ESI) available: Optimized geometries, identified isomers, calculated VDEs, ADEs, RMSDs, BEs, and EDA analysis.

hydrophilic outer surfaces are well-known as remarkable drug delivery agents,<sup>23-25</sup> and preliminary tests indicate that they are suitable to promote the transport of  $B_{12}X_{12}^{2-}$  into the cells.<sup>22</sup> The  $\alpha$ -CD,  $\beta$ -CD, and  $\gamma$ -CD are a class of macrocyclic oligosaccharides consisting of 6, 7, and 8 chair-like D-glucopyranoside units, respectively. There are three free hydroxyls in each glucopyranoside unit, of which one primary and two secondary hydroxyls are located on the small and wide openings of the cavities, respectively. The CDs are also demonstrated to be remarkable hydrophobic binding pocket for different sized anions, preferentially the chaotropic anions of the original Hofmeister series<sup>26</sup>,  $I_3^{-}$ <sup>27</sup> and the classical Keggin POM ion ( $PMO_{12}O_{40}^{3-}$ )<sup>28</sup>. The strong affinity of dodecaborate clusters with the CDs in aqueous solution<sup>29, 30</sup> was attributed to the chaotropic effect<sup>22, 30, 31</sup>. The chaotropic effect is the result of the significant recovery of the H-bonded water networks upon the relocation of the chaotropic dodecaborate dianions from the aqueous bulk into the nonpolar binding pocket. However, the chaotropic effect cannot play a role in the gas phase where the isolated species don't interact with the surroundings. Therefore, it is significant to study the intrinsic properties of the binding effect between dodecaborate dianions and the CDs in the gas phase complementary to the studies in the condensed phase.

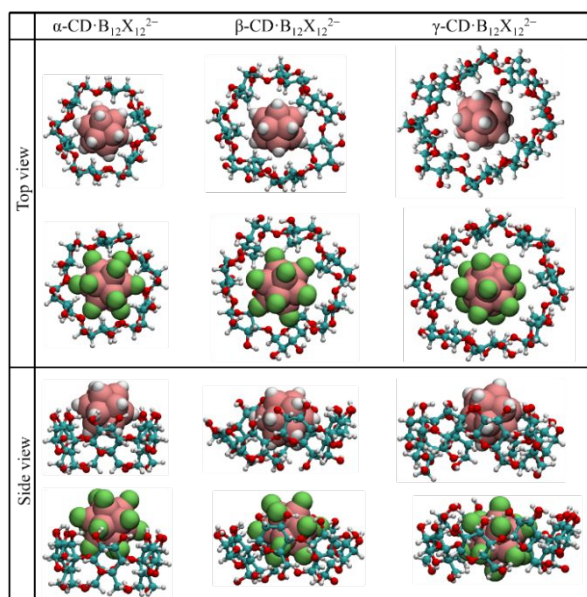


**Fig. 1** The optimized geometries of CDs- $B_{12}X_{12}^{2-}$  ( $X = H$  and  $F$ ) with the top view (upper panel) and side view (lower panel). The  $B_{12}X_{12}^{2-}$  dianions are shown with Stuart model ( $H$  in white and  $F$  in green) and CDs are displayed with ball-stick models with  $H$ ,  $O$ , and  $C$  atoms in white, red, and turquoise, respectively.

In this work, a series of gas-phase  $\chi$ -CD- $B_{12}X_{12}^{2-}$  ( $\chi = \alpha$ -,  $\beta$ -,  $\gamma$ ;  $X = H, F$ ) dianion complexes (see Fig. 1) were transferred into the gas phase via electrospray ionization, and their electronic structures were experimentally determined using negative ion photoelectron spectroscopy (NIPES). Experimentally-determined vertical detachment energies (VDEs) and adiabatic detachment energies (ADEs) are directly derived from the NIPES

spectra. Quantum chemical calculations were carried out to explore different low-lying isomeric geometries, to calculate electron binding energies (EBEs), host-guest binding energies (BEs), and to analyze molecular orbitals, and the nature of noncovalent interactions of the  $\chi$ -CD- $B_{12}X_{12}^{2-}$  complexes. The obtained knowledge about electronic stability, size-, and molecular specific noncovalent interactions are valuable molecular level information, which may contribute to the design of new boron compound delivery agents for applications in BNCT.

## 2. Experimental methodology and computational details

**Negative ion photoelectron spectroscopy (NIPES) experiments.** The experiments were carried out using the PNNL size-selected NIPES apparatus that consists of an electrospray ionization source, a cryogenic ion trap, and a magnetic bottle time-of-flight photoelectron spectrometer<sup>32</sup>. The spraying solutions were prepared by mixing the potassium salts solutions of  $B_{12}H_{12}^{2-}$  and  $B_{12}F_{12}^{2-}$  (0.1 mM using 1/3  $H_2O/CH_3OH$  solvent mixture) with the CD solutions (0.1 mM using  $CH_3OH$  solvent) at the ratio of 1:3 and 1:10, respectively. The CD- $B_{12}X_{12}^{2-}$  complexes produced were guided by two RF-only quadrupoles and directed into the cryogenic Paul trap set at 20 K, where they were accumulated and thermalized for 20-100 ms by collisions with a cold buffer gas (20%  $H_2$  balanced in helium) to eliminate the hot bands and improve the spectral energy resolution. Then, the cryogenically cooled anions were pulsed out into the extraction zone of a TOF mass spectrometer for the mass-to-charge separation and analysis. The desired  $\chi$ -CD- $B_{12}X_{12}^{2-}$  complexes were mass-selected and maximally decelerated before being photodetached with the 157 nm (7.866 eV) photons from an F2 excimer laser. The detached photoelectrons were collected with almost 100% efficiency by the magnetic bottle and analyzed in a 5.2 m long electron flight tube. The laser was operated at 20 Hz with the ion beam off at alternating laser shots, affording shot-to-shot background subtraction. Those obtained TOF spectra were converted to the electron kinetic energy spectra, calibrated with the known spectra of  $I^-$  and  $Au(CN)_2^-$ . The electron binding energy (EBE) spectra were obtained by subtracting the kinetic energies from the detachment photon energy. The energy resolution was approximately 20 meV (full width at half maximum) for electrons with 1 eV kinetic energy.

**Computational details.** Hundreds of molecular configurations were initially generated using the Molclus<sup>33</sup> code, followed by preliminarily semi-empirical optimization at the PM6-DH+<sup>34</sup> level using MOPAC program.<sup>35</sup> About 40 low-lying isomers of CDs- $B_{12}X_{12}^{2-}$  ( $X = H, F$ ) complexes were selected and optimized at the B3LYP<sup>36, 37</sup>-D3(BJ)<sup>38</sup>/6-31G(d)<sup>39, 40</sup> level and these isomers are sorted again by energy at the present optimization level. And at least 10 low-lying isomers were selected to re-optimize at the M062X<sup>41</sup>-D3<sup>42</sup>/6-311G(d,p)<sup>43-45</sup> level to ensure the lowest-lying geometries shown in Fig. 1 being identified. Optimization using the mixed basis set (anionic  $B_{12}X_{12}^{2-}$  ( $X = H, F$ ) with 6-311+G(d,p) and neutral  $\alpha$ -CD with 6-311G(d,p)) were

performed, showing negligible effect by adding diffuse functions (see details in the ESI†). The self-consistent-field (SCF) energies of the optimized  $B_{12}X_{12}^{2-}$ ,  $CDs \cdot B_{12}X_{12}^{2-}$  and their corresponding monoanions were obtained at the M062X-D3/6-311+G(d,p)<sup>44-47</sup> level. The theoretical vertical detachment energies (VDEs) were determined as the energy differences between the corresponding monoanions and dianions both at the dianions' optimized geometries, and the theoretical adiabatic detachment energies (ADEs) were obtained as the energy difference between the corresponding monoanions and dianions based on their respective optimized geometries with zero-point energy (ZPE) corrections. For comparison, the geometry optimization and single point energy calculation were also carried out using the PBE0<sup>48</sup> functional with the D3(BJ) dispersion correction as shown in Tab. S2 in the ESI†. The intermolecular interaction energies, i.e., binding energies (BEs) between  $B_{12}X_{12}^{2-}$  and CDs, were calculated as the energy differences between the energies of the  $CDs \cdot B_{12}X_{12}^{2-}$  complexes and the sum of the energies of  $B_{12}X_{12}^{2-}$  and CDs with the basis set superposition error (BSSE) corrections using the counterpoise method of Boys and Bernardi<sup>49</sup>. To give an intuitive understanding of the noncovalent interactions in the  $CDs \cdot B_{12}X_{12}^{2-}$  complexes, an independent Gradient Model (IGM)<sup>50, 51</sup> analysis based on the electron density gradient employing pro-molecular density was performed using the Multiwfn code<sup>52</sup>. This model can provide a visual expression on the noncovalent interactions in molecular systems. The energy decomposition analysis was further performed by the symmetry adapted perturbation theory (SAPT) at the SAPT0/jun-cc-pVDZ level<sup>53-55</sup> using PSI4 code<sup>56</sup> and based on AMBER force field<sup>57</sup> (B atom based on UFF force field<sup>58</sup>), respectively. All the DFT calculations were carried out with the Gaussian 16 software<sup>59</sup>.

### 3. Photoelectron spectra of $B_{12}X_{12}^{2-}$ and $CDs \cdot B_{12}X_{12}^{2-}$ ( $X = H, F$ )

The 20 K 157 nm NIPE spectra of  $B_{12}H_{12}^{2-}$  and its  $\alpha$ -,  $\beta$ -,  $\gamma$ -CD complexes are shown in Fig. 2 (a-d), and the corresponding  $B_{12}F_{12}^{2-}$  spectra are presented in Fig. 2 (e-h), respectively. Compared to bare  $B_{12}X_{12}^{2-}$ , all complex spectra exhibit significant blue shifts in EBE, broader and less resolved spectral bands with new intense bands emerged starting at  $\sim 1.5$  eV above the first spectral features. The experimental VDEs were measured from the maximum of the first spectral band in each spectrum, while the experimental ADEs were estimated from the spectral onset threshold plus the instrumental resolution as indicated by the gray dashed and dotted lines, respectively. As shown in Fig. 2 and listed in Tab. 1, the binding interactions between the CD cavities and  $B_{12}X_{12}^{2-}$  greatly stabilize the  $B_{12}X_{12}^{2-}$  dianions electronically. Compared to the free  $B_{12}H_{12}^{2-}$  dianion, the VDE increases by 2.40, 2.75, and 2.70 eV for  $\alpha$ -,  $\beta$ -, and  $\gamma$ -CD- $B_{12}H_{12}^{2-}$ , respectively; while the corresponding VDE increases for the  $B_{12}F_{12}^{2-}$  case are 2.10, 2.43, and 2.40 eV, respectively. Similar ADE increases upon clustering  $B_{12}X_{12}^{2-}$  with CDs are observed, i.e., 2.27, 2.67, 2.67 eV for  $\alpha$ -,  $\beta$ -, and  $\gamma$ -

CD- $B_{12}H_{12}^{2-}$ , and 1.90, 2.25, and 2.15 eV for  $\alpha$ -,  $\beta$ -, and  $\gamma$ -CD- $B_{12}F_{12}^{2-}$ , respectively. It can be seen that each CD stabilizes  $B_{12}H_{12}^{2-}$  ca. 0.3 eV more than  $B_{12}F_{12}^{2-}$ , and  $\beta$ -CD and  $\gamma$ -CD exhibit similar stabilization. Both are  $\sim 0.3$  eV larger than that of  $\alpha$ -CD. The absolute VDEs and ADEs of all  $CDs \cdot B_{12}F_{12}^{2-}$  complexes are larger than those of the corresponding  $CDs \cdot B_{12}H_{12}^{2-}$  by  $\sim 0.5$  eV. Therefore, it is evident that the intermolecular interactions between CD and  $B_{12}X_{12}^{2-}$  strongly depend on the host size ( $\alpha$ ,  $\beta$ ,  $\gamma$ ) and guest identity ( $X = H$  or  $F$ ).

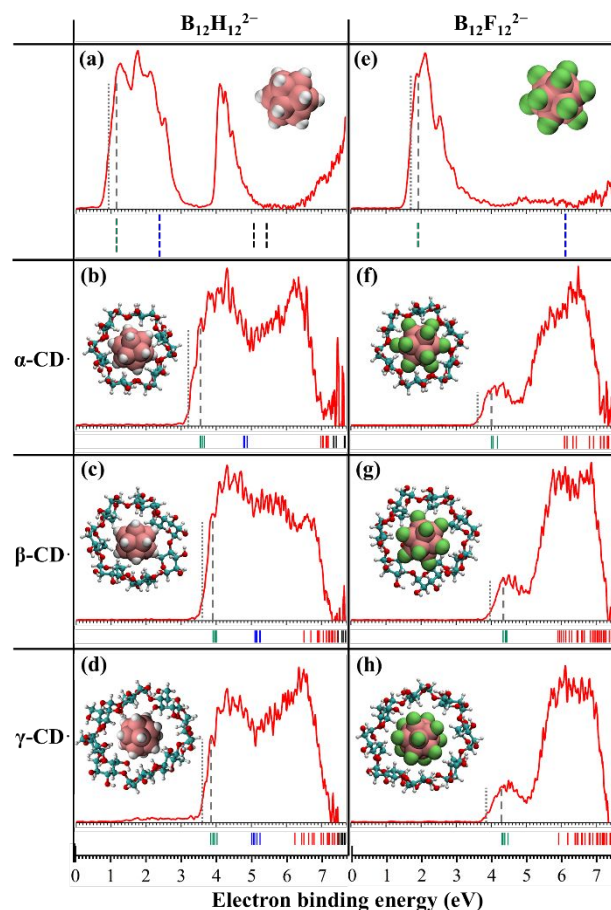


**Fig. 2** The measured NIPE spectra of (a)  $B_{12}H_{12}^{2-}$ , (b)  $\alpha$ -CD- $B_{12}H_{12}^{2-}$ , (c)  $\beta$ -CD- $B_{12}H_{12}^{2-}$ , (d)  $\gamma$ -CD- $B_{12}H_{12}^{2-}$ , (e)  $B_{12}F_{12}^{2-}$ , (f)  $\alpha$ -CD- $B_{12}F_{12}^{2-}$ , (g)  $\beta$ -CD- $B_{12}F_{12}^{2-}$ , (h)  $\gamma$ -CD- $B_{12}F_{12}^{2-}$  taken with 157 nm (7.866 eV) photons. The gray dashed and dotted lines designate the spectral EBE positions from which the VDEs and ADEs are determined, respectively. The short color-coded bars below the spectra of bare  $B_{12}X_{12}^{2-}$  denote the highly degenerate Hartree-Fock (HF) occupied molecular orbitals (MOs). The color-coded short vertical bars below each  $\chi$ -CD- $B_{12}X_{12}^{2-}$  spectrum denote the pseudo-degenerated HF MOs density of states (DOS) spectra. The green, blue, and red solid bars represent the MOs dominated by boron-centered orbitals, boron and hydrogen/fluorine mixed orbitals, and oxygen orbitals in CDs, respectively. The DOS plots were obtained by shifting orbital energies to lower EBE so that the HOMO energy fits the the experimental VDEs<sup>60</sup>.

## ARTICLE

**Tab. 1** The experimental and calculated VDEs and ADEs (in eV) of  $B_{12}X_{12}^{2-}$  and CDs- $B_{12}X_{12}^{2-}$  (X = H, F) at the M062X-D3/6-311+G(d,p) level. The experimental  $\Delta$ VDEs and the calculated BEs (in eV) between the  $B_{12}X_{12}^{2-}$  dianions and CDs are also listed for comparison. The mean absolute deviations (MADs) of calculated VDEs and ADEs for CDs- $B_{12}X_{12}^{2-}$  are shown with respect to the corresponding experimental values.

	VDE		ADE		$\Delta$ VDE (Expt.)	BE (Calc.)
	Expt.	Calc.	Expt.	Calc.		
$B_{12}H_{12}^{2-}$	$1.15 \pm 0.05$	1.44	$0.93 \pm 0.05$	1.04	-	-
$B_{12}F_{12}^{2-}$	$1.90 \pm 0.05$	2.43	$1.70 \pm 0.05$	1.70	-	-
$\alpha$ -CD- $B_{12}H_{12}^{2-}$	$3.55 \pm 0.10$	3.17	$3.20 \pm 0.10$	2.55	2.40	3.65
$\beta$ -CD- $B_{12}H_{12}^{2-}$	$3.90 \pm 0.10$	3.96	$3.60 \pm 0.10$	3.27	2.75	5.28
$\gamma$ -CD- $B_{12}H_{12}^{2-}$	$3.85 \pm 0.10$	4.16	$3.60 \pm 0.10$	3.24	2.70	5.57
$\alpha$ -CD- $B_{12}F_{12}^{2-}$	$4.00 \pm 0.10$	4.06	$3.60 \pm 0.10$	3.31	2.10	3.10
$\beta$ -CD- $B_{12}F_{12}^{2-}$	$4.33 \pm 0.10$	4.76	$3.95 \pm 0.10$	3.79	2.43	4.64
$\gamma$ -CD- $B_{12}F_{12}^{2-}$	$4.30 \pm 0.10$	4.67	$3.85 \pm 0.10$	3.90	2.40	4.50
MAD		0.27		0.31		

## 4. Theoretical results and discussion

### 4.1 Geometric structures of CDs- $B_{12}X_{12}^{2-}$ (X = H and F)

The geometries of isolated  $B_{12}X_{12}^{2-}$  and  $\alpha$ -,  $\beta$ -,  $\gamma$ -CD were optimized at the M062X-D3/6-311G(d,p) level and are shown in the ESI† (Fig. S1). Both  $B_{12}H_{12}^{2-}$  and  $B_{12}F_{12}^{2-}$  possess regular icosahedral structures, in accord with the previous studies<sup>20, 21</sup>. The cavity of the free CD molecule becomes larger with increasing glucopyranoside units. Fig. 1 displays the optimized geometries of  $\alpha$ -,  $\beta$ -,  $\gamma$ -CD- $B_{12}X_{12}^{2-}$  (X = H and F) complexes, obtained at the M062X-D3/6-311G(d,p) level. It is evident that the  $B_{12}X_{12}^{2-}$  dianions are embedded into the wider openings of various CDs at different depths. The embedding extents, i.e., the deviation from total inclusion, defined as the distances between the centroids of two fragments, are calculated as 3.14, 1.57, 0.12 Å for  $\alpha$ -,  $\beta$ -,  $\gamma$ -CD- $B_{12}H_{12}^{2-}$ , and 3.55, 1.99, 0.12 Å for  $\alpha$ -,  $\beta$ -,  $\gamma$ -CD- $B_{12}F_{12}^{2-}$ , respectively. Clearly, the  $B_{12}X_{12}^{2-}$  guest is inserted into the CD host increasingly deeper from  $\alpha$  to  $\beta$  and to  $\gamma$ . The strong interactions between  $B_{12}X_{12}^{2-}$  and CDs are inevitably accompanied by the distortions of the geometries of each fragment. In order to quantitatively characterize the overall deformation of geometries for the free  $B_{12}X_{12}^{2-}$  dianions vs.  $B_{12}X_{12}^{2-}$  in CDs- $B_{12}X_{12}^{2-}$  and the free CDs vs. CDs in CDs- $B_{12}X_{12}^{2-}$ , the index of root mean square displacement (RMSD) is calculated according to the following equation:

$$\text{RMSD} = \sqrt{\frac{1}{N} \sum_i^{n \text{ atoms}} [(x_i - x'_i)^2 + (y_i - y'_i)^2 + (z_i - z'_i)^2]}$$

where  $x$ ,  $y$  and  $z$  denote the coordinates of atoms in the optimized geometries. The calculated RMSDs are shown in Tab. S1 in ESI†. The RMSDs of  $B_{12}X_{12}^{2-}$  are among 0.018 to 0.066 Å, suggesting that the geometries of the  $B_{12}X_{12}^{2-}$  dianions remain almost unchanged after binding with the CD hosts. The geometries of CDs change significantly with much larger RMSDs of 0.150 to 1.473 Å. The larger the size of the CD is, the more significant geometric distortion of CD will occur after binding with the  $B_{12}X_{12}^{2-}$  guest. This is easily understood by the fact that the flexibility of CDs increases with their size, and their shape is sensitive to the interactions with the very rigid  $B_{12}X_{12}^{2-}$  dianions.

### 4.2 Calculated VDEs, ADEs, and intermolecular BEs

In order to make a direct comparison to the experimental results, the theoretical VDEs, ADEs are calculated at the M062X-D3/6-311G+(d,p) level, and are listed in Tab. 1. For  $B_{12}X_{12}^{2-}$  (X = H, F), their theoretical VDEs and ADEs were calculated using highly correlated Coupled Cluster with Single, Double and a perturbative estimate of Triple excitations [CCSD(T)] and IP/EA-EOMCCSD methods in two previous publications<sup>20, 21</sup>, and the

values obtained agreed excellently with the experimental results. However, the extremely high computational cost of CCSD(T) and IP/EA-EOMCCSD methods prevents their application to the large complex systems studied in this work. Alternatively, the M062X functional, which has been demonstrated its superiority in non-covalent interaction systems,<sup>61</sup> provides a good balance between accuracy of the results and computational cost. As shown in Tab. 1, compared to the experimental data, the mean absolute deviations (MADs) of the calculated VDEs and ADEs of CDs·B<sub>12</sub>X<sub>12</sub><sup>2-</sup> are 0.27 eV and 0.31 eV, respectively, indicating the theoretical results are in overall good agreement with the trends of experimental measurements. The reliability of the current method (i.e. M062X functional) for  $\chi$ -CD·B<sub>12</sub>X<sub>12</sub><sup>2-</sup> complexes was confirmed with the slightly smaller mean absolute errors (MAD = 0.25 eV) with respect to the experimental data by comparing with the results from the popular PBE0 functional (MAD = 0.29 eV) in Tab. S2. Besides the global minimum, low-lying isomers of each complex were also identified, and their VDEs and the index of root mean square displacements (RMSDs) compared with the lowest-lying structures are listed in Tab. S3. The VDEs of different low-lying isomers are close to that of the lowest-lying structures from 0.07 eV to 0.41 eV with the RMSDs of 0.002 to 0.37 Å. The results indicate that these low-lying isomers may coexist in the experiments and contribute to the broadness of the CDs·B<sub>12</sub>X<sub>12</sub><sup>2-</sup> spectra, albeit the fact that the low temperature tends to suppress entropic effects which might be crucial for flexible molecules like CD at room temperature.

As shown in Tab. 1, the intermolecular binding strength between  $\alpha$ -,  $\beta$ -,  $\gamma$ -CD and B<sub>12</sub>H<sub>12</sub><sup>2-</sup> are 3.65, 5.28 and 5.57 eV, respectively. These corresponding values for the CDs with B<sub>12</sub>F<sub>12</sub><sup>2-</sup> are 3.10, 4.64, 4.50 eV and therefore smaller. They are in the range of 3.10 to 5.57 eV, that are significantly larger than the corresponding experimental  $\Delta$ VDE values (2.10 to 2.75 eV).

Estimation of the binding energy of a neutral molecule N with an anion A<sup>n-</sup> based on NIPES spectra has been reported before.<sup>62,63</sup> A lower limit of the binding energy can be estimated from the EBE increase of N·A<sup>n-</sup> complex relative to the EBE of A<sup>n-</sup>, if the interaction energy between N and A<sup>(n-1)-</sup> is negligible (see Fig. S2 in ESI†). This condition can be reasonably fulfilled if the anion is singly charged (n=1). However, [B<sub>12</sub>X<sub>12</sub>]<sup>2-</sup> ions are doubly charged and the interaction energy between the CDs and the incorporated anion [B<sub>12</sub>X<sub>12</sub>]<sup>•-</sup> is substantial. The calculated binding energies between CDs and [B<sub>12</sub>X<sub>12</sub>]<sup>•-</sup> at the same DFT level amount to 1.4 to 2.8 eV (i.e., 1.91, 2.76, 2.85 eV, and 1.41, 2.26, 2.24 eV for  $\alpha$ -,  $\beta$ -,  $\gamma$ -CD interacting with [B<sub>12</sub>H<sub>12</sub>]<sup>•-</sup> and [B<sub>12</sub>F<sub>12</sub>]<sup>•-</sup>, respectively, Tab. S4). Therefore, the EBE increases are considerably smaller than the binding energies of CDs with [B<sub>12</sub>X<sub>12</sub>]<sup>2-</sup> dianions as shown in Tab. 1. It should be pointed out that although the absolute numbers are different, the trend of  $\Delta$ EBEs, obtained from the experiments, does parallel the trend of the calculated binding energies (Tab.1). Therefore the NIPES experiments are able to make qualitative suggestions on how well the guest molecules fit in the host cavities: the better the structural match is, the higher the binding energies (or  $\Delta$ EBEs) will be.

### 4.3 Molecular orbitals analyses

The NIPE spectral bands can be qualitatively revealed as successive removals of electrons from the frontier occupied MOs in light of Koopmans' theorem<sup>64</sup>. It is instructive to compare the resulting density of states (DOS) of the anion to the observed spectrum. The DOS of B<sub>12</sub>X<sub>12</sub><sup>2-</sup> dianions and  $\chi$ -CD·B<sub>12</sub>X<sub>12</sub><sup>2-</sup> complexes are calculated at the HF/6-311+G(d,p) level and shown in Fig. 2. The MOs of isolated B<sub>12</sub>X<sub>12</sub><sup>2-</sup> are highly degenerated due to their icosahedral (I<sub>h</sub>) symmetry as shown in Fig. 2 (a) and (e). The binding of CDs breaks the I<sub>h</sub> symmetry of B<sub>12</sub>X<sub>12</sub><sup>2-</sup>. As a consequence, the degenerated orbitals split up in energy. As shown in the shifted DOS spectra (Fig.2 (b-d) and (f-h)), the groups of MOs at the position of HOMOs were pseudo-degenerated within 0.18 eV for CDs·B<sub>12</sub>H<sub>12</sub><sup>2-</sup> and 0.17 eV for CDs·B<sub>12</sub>F<sub>12</sub><sup>2-</sup>. The HOMO-1 locates far away from the HOMO for B<sub>12</sub>F<sub>12</sub><sup>2-</sup> with a difference of 4.21 eV, while a much closer energetic difference (1.24 eV) between HOMO and HOMO-1 is observed for B<sub>12</sub>H<sub>12</sub><sup>2-</sup>. A similar case is also found in the  $\chi$ -CD·B<sub>12</sub>H<sub>12</sub><sup>2-</sup> complexes, where pseudo-degenerated HOMO-1 and HOMO are derived from the borate with the energy differences of 0.99 to 1.12 eV. For CD·B<sub>12</sub>F<sub>12</sub><sup>2-</sup> complexes, the situation changes with the HOMO-1 MOs derived from the oxygen p orbitals from CDs, at the energy level of 1.45 to 1.91 eV deeper than the pseudo HOMO.

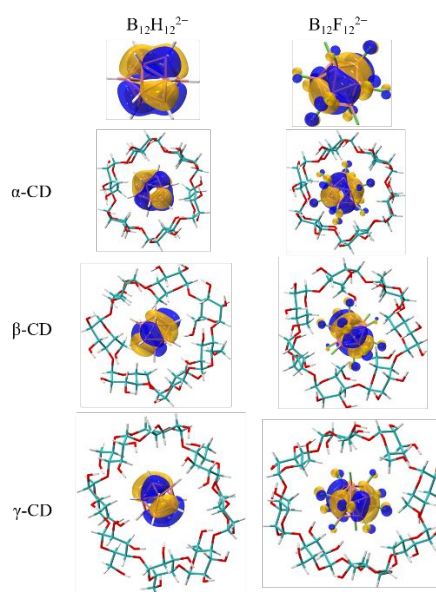


**Fig. 3** The plots for highest occupied molecular orbitals (HOMOs) of B<sub>12</sub>X<sub>12</sub><sup>2-</sup> and CDs·B<sub>12</sub>X<sub>12</sub><sup>2-</sup> (X = H, F) (isovalue = 0.03).

Fig. 3 and Fig. S3 show the corresponding frontier molecular orbitals for B<sub>12</sub>X<sub>12</sub><sup>2-</sup> dianions and  $\chi$ -CD·B<sub>12</sub>X<sub>12</sub><sup>2-</sup> complexes. Both HOMOs of B<sub>12</sub>H<sub>12</sub><sup>2-</sup> and B<sub>12</sub>F<sub>12</sub><sup>2-</sup> are boron-centered while there is also small contribution from the fluorine shell to the HOMO for B<sub>12</sub>F<sub>12</sub><sup>2-</sup>. The plots of the sets of highest lying orbitals of CDs·B<sub>12</sub>X<sub>12</sub><sup>2-</sup> (within 0.3 eV of the HOMO) do appear similar to the highly degenerate HOMO of the corresponding bare B<sub>12</sub>X<sub>12</sub><sup>2-</sup> dianions, suggesting that the

photoelectrons corresponding to the first spectral bands are mainly detached from the inner boron-centered cores (corresponding to the green vertical bars in the DOS spectra in Fig. 2). The second set of orbitals of CDs·B<sub>12</sub>H<sub>12</sub><sup>2-</sup> predominately consists of boron and hydrogen-mixed orbitals (blue vertical bars) and the further lower-lying MOs correspond to the oxygen occupied orbitals from CDs (red vertical bars). However, in the case of CDs·B<sub>12</sub>F<sub>12</sub><sup>2-</sup>, all lower-lying MOs than those associated with the highly degenerate HOMO in the bare ion are mainly composed of the CD oxygen occupied orbitals (See Fig. S4). The much larger HOMO and HOMO-1 energy separation in CDs·B<sub>12</sub>F<sub>12</sub><sup>2-</sup> (1.45 to 1.91 eV) than that in CDs·B<sub>12</sub>H<sub>12</sub><sup>2-</sup> (0.99 to 1.12 eV) and the fact that HOMO-1 in the former consists of the oxygens of CDs, while of the boron core in the latter, provide a qualitative explanation for observing a well-defined 1<sup>st</sup> spectral band in the former while an intense and less-resolved band for the latter. In both cases, the spectral bands at high EBE are primarily attributed to the ionization on oxygens occurring on CDs. It is worth noting that the energy of highest lying CD orbitals (red vertical bars) for CDs·B<sub>12</sub>F<sub>12</sub><sup>2-</sup> (< 6 eV) is smaller than that for CDs·B<sub>12</sub>H<sub>12</sub><sup>2-</sup> (> 6 eV) (Fig.2). This is due to the fact that the more negative charges are accumulated in the F shell in the former than the H shell in the latter shown in Fig. S5. The more negative charges on the ligand shell will push up the O orbital level from CD. Therefore the experimental spectrum is not only able to indicate how strong the host-guest interaction, as discussed above in section 4.2, but also encodes direct electronic structure information and charge distribution of the complex.

#### 4.4 The noncovalent interaction between B<sub>12</sub>X<sub>12</sub><sup>2-</sup> (X = H, F) and various CDs

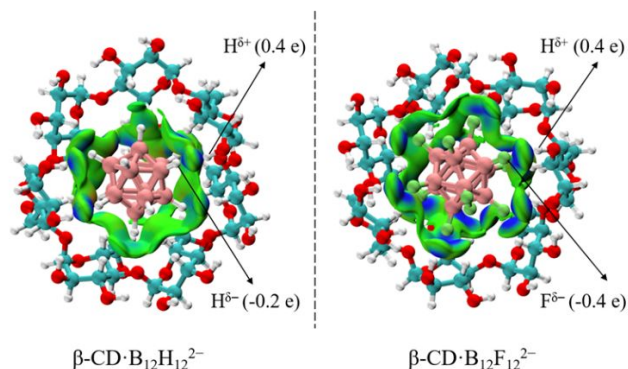


**Fig. 4** The  $\delta g^{\text{inter}} = 0.005$  a.u. isosurfaces for  $\beta\text{-CD}\cdot\text{B}_{12}\text{X}_{12}^{2-}$  (X = H, F) colored according to a blue-green-red scheme over the range  $-0.05 < \text{sign}(\lambda_2)\rho < 0.05$  a.u., where the blue, green, and red isosurfaces represent the strong attractions, weak attractions, and strong repulsions, respectively. The charges of H-bonding action sites in  $\beta\text{-CD}\cdot\text{B}_{12}\text{X}_{12}^{2-}$  (X = H, F) show the formation of unconventional dihydrogen bonding O-H<sup>δ+</sup>...H<sup>δ-</sup>-B for X = H and conventional O-H...F-B hydrogen bonding interaction for X = F (the negative charges of B<sub>12</sub>X<sub>12</sub><sup>2-</sup> in  $\beta\text{-CD}\cdot\text{B}_{12}\text{X}_{12}^{2-}$  (X = H, F) were not evenly distributed by reason of the influence of hosts). The isosurfaces for all complexes are given in Fig. S6.

An intuitive, semi-quantitative estimation of the intermolecular interaction between B<sub>12</sub>X<sub>12</sub><sup>2-</sup> and CDs can be obtained by the independent gradient model (IGM), affording analysis of the noncovalent interactions, especially for the large-size host-guest molecular systems.<sup>65, 66</sup> In the IGM analysis, the intermolecular interaction can be divided into three types according to their strength of interactions: strong attractions with high electrostatic character such as H-bonding interactions, weak van der Waals interactions such as dispersion interaction, and strong repulsions such as those due to steric effects. To give a quantitative estimation of electrostatic vs. non-electrostatic interactions, the energy decomposition analyses (EDA) based on the SAPT0 approach and molecular force field (FF) are employed. As shown in Tab. S5, the total intermolecular interaction ( $E_{\text{tot}}$ ) obtained by the EDA approaches are qualitatively consistent with the above DFT BE calculations, that is,  $E_{\text{tot}}$  of  $\beta\text{-CD}\cdot\text{B}_{12}\text{X}_{12}^{2-}$  and  $\gamma\text{-CD}\cdot\text{B}_{12}\text{X}_{12}^{2-}$  is significantly larger than that of  $\alpha\text{-CD}\cdot\text{B}_{12}\text{X}_{12}^{2-}$ , and for a given CD host,  $E_{\text{tot}}$  of the B<sub>12</sub>H<sub>12</sub><sup>2-</sup> complex is larger than that of the B<sub>12</sub>F<sub>12</sub><sup>2-</sup> complex. In addition, as shown in Fig. 4 and Fig. S6, the IGM model validates the obvious existence of strong electrostatic attractions (blue) and van der Waals interactions (green) in  $\chi\text{-CD}\cdot\text{B}_{12}\text{X}_{12}^{2-}$  complexes. The visualization clearly indicates the formation of O-H...F-B hydrogen bonding in CDs·B<sub>12</sub>F<sub>12</sub><sup>2-</sup>, in which B<sub>12</sub>F<sub>12</sub><sup>2-</sup> is identified as the acceptor (due to the electronegativity of F atom) and CDs as the H atom donor. Interestingly, Fig. 4 illustrates the formation of B-H...H-O dihydrogen bonds that contribute significantly to the binding mode of  $\chi\text{-CD}\cdot\text{B}_{12}\text{H}_{12}^{2-}$ . The dihydrogen bonding, also called hydridic-to-protonic interaction, has been found and characterized by infrared, crystallography, and theoretical approaches in boron coordination compounds.<sup>67-72</sup> The charge distribution using a grid-based method (CHELPG) in Fig. 4 and Fig. S5 has confirmed the formation of dihydrogen bonding between H<sup>δ+</sup> donors from  $\chi\text{-CD}$  and H<sup>δ-</sup> acceptors in B<sub>12</sub>H<sub>12</sub><sup>2-</sup> (for the isolated B<sub>12</sub>H<sub>12</sub><sup>2-</sup>, the negative charges are localized on H atoms<sup>21</sup>).

We want to emphasize that electrostatic interaction plays a dominant role in all cases of CDs·B<sub>12</sub>X<sub>12</sub><sup>2-</sup> (X = H, F). For example, with respect to  $\beta\text{-CD}\cdot\text{B}_{12}\text{X}_{12}^{2-}$ , the electrostatic term of  $\beta\text{-CD}\cdot\text{B}_{12}\text{H}_{12}^{2-}$  is close to  $\beta\text{-CD}\cdot\text{B}_{12}\text{F}_{12}^{2-}$  (within 0.09 eV by SAPT0 vs. 0.07 eV by FF) (Tab. S5). This may be surprising because F—H interactions are intuitively assumed to have a strong electrostatic nature. A similar high value in the energy decomposition analysis for the  $\beta\text{-CD}\cdot\text{B}_{12}\text{H}_{12}^{2-}$  complex may be rationalized (i) by exceptionally strong hydridic-to-protonic interaction and (ii) the smaller size of the doubly charged ion, which generally results in stronger electrostatic attractions with the polar  $\beta\text{-CD}$  molecule. Moreover, the total interaction energy of  $\beta\text{-CD}\cdot\text{B}_{12}\text{H}_{12}^{2-}$  is 0.75 eV (SAPT0) vs. 0.63 eV (FF) larger than  $\beta\text{-CD}\cdot\text{B}_{12}\text{F}_{12}^{2-}$ , mainly owing to the enhanced dispersion and induction terms. The reason why there is more contributions from the dispersion and induction terms in  $\beta\text{-CD}\cdot\text{B}_{12}\text{H}_{12}^{2-}$  than in  $\beta\text{-CD}\cdot\text{B}_{12}\text{F}_{12}^{2-}$  is primarily due to the larger polarizability of the former than the latter (741.09 a.u. for  $\beta\text{-CD}\cdot\text{B}_{12}\text{H}_{12}^{2-}$  vs. 715.75 a.u. for  $\beta\text{-CD}\cdot\text{B}_{12}\text{F}_{12}^{2-}$  and 164.61 a.u. for B<sub>12</sub>H<sub>12</sub><sup>2-</sup> vs 130.98 a.u.

for  $B_{12}F_{12}^{2-}$  obtained at the M062X-D3/6-311+G(d,p) level, Tab. S6).

## 5. Conclusions

Herein, we reported a joint experimental and computational study on the geometric, electronic structures and noncovalent interactions of  $\chi$ -CD· $B_{12}X_{12}^{2-}$  (X = H, F) dianion complexes. On the one hand, for a given  $B_{12}X_{12}^{2-}$ , the EBEs of  $\beta$ -CD· $B_{12}X_{12}^{2-}$  and  $\gamma$ -CD· $B_{12}X_{12}^{2-}$  are similar, both being significantly larger than that of  $\alpha$ -CD· $B_{12}X_{12}^{2-}$ . On the other hand, for a given CD, the EBE of the  $B_{12}F_{12}^{2-}$  complex is larger than that of the corresponding  $B_{12}H_{12}^{2-}$  complex. Furthermore, the noncovalent interactions between CD and  $B_{12}H_{12}^{2-}$  is appreciably larger than that between CD and  $B_{12}F_{12}^{2-}$ . The above detailed information clearly shows size- and molecular specific effects on the electronic stability and noncovalent interactions in CDs· $B_{12}X_{12}^{2-}$ . The formation of specific dihydrogen bonding interaction in CDs· $B_{12}H_{12}^{2-}$  and its stabilization is particularly worth noting.

The theoretical calculations are overall in good agreement with the experimental results. The most loosely bound electrons are derived from the boron cage orbitals in the  $\chi$ -CD· $B_{12}X_{12}^{2-}$  complexes. The calculated BE values of CDs· $B_{12}X_{12}^{2-}$  are found to be significantly larger than the experimental  $\Delta$ VDE values, which can be attributed to the non-negligible BEs between the  $B_{12}X_{12}^{2-}$  monoanions and CDs. The IGM and energy decomposition analysis confirm the formations of two types of hydrogen bonds, i.e., B-H...H(O) dihydrogen bonds in CDs· $B_{12}H_{12}^{2-}$  and O-H...F-B bonds in CDs· $B_{12}F_{12}^{2-}$ . The analyses further indicate the electrostatic term plays a dominant role in the noncovalent interaction for the CDs· $B_{12}X_{12}^{2-}$  complexes, and the bigger contribution from the dispersion and induction terms is mainly responsible for the larger total interactions found in CDs· $B_{12}H_{12}^{2-}$  than those in CDs· $B_{12}F_{12}^{2-}$ .

## Conflicts of interest

There are no conflicts to declare.

## Acknowledgements

The NIPES experiments done at PNNL were supported by the U.S. Department of Energy (DOE), Office of Science, Office of Basic Energy Sciences, Division of Chemical Sciences, Geosciences and Bioscience (X.-B.W. and Q.Y.) and was performed at the EMSL, a national scientific user facility sponsored by DOE's Office of Biological and Environmental Research and located at Pacific Northwest National Laboratory. H.S. and Z.S. acknowledge the funding support of National Natural Science Foundation of China (Nos.11727810, 61720106009 and 21603074), the Science and Technology Commission of Shanghai Municipality (Nos. 19JC1412200), and the Program of Introducing Talents of Discipline to Universities 111 project (B12024). Z. L. thanks the China Scholarship Council (CSC) for financial support. We acknowledge the ECNU

Multifunctional Platform for Innovation (001) and HPC Research Computing Team for providing computational and storage resources. J.W. acknowledges support from the Alexander von Humboldt foundation (Feodor Lynen Fellowship and Rückkehrerstipendium), a Freigeist fellowship of the Volkswagenfoundation and Prof. Vladimir A. Azov for helpful discussions.

## Notes and references

- H. C. Longuet-Higgins, M. D. V. Roberts and H. J. Emeleus, *Proc. R. Soc. Lond. A.*, 1955, **230**, 110-119.
- A. R. Pitochelli and F. M. Hawthorne, *J. Am. Chem. Soc.*, 1960, **82**, 3228-3229.
- S. V. Ivanov, S. M. Miller, O. P. Anderson, K. A. Solntsev and S. H. Strauss, *J. Am. Chem. Soc.*, 2003, **125**, 4694-4695.
- V. Geis, K. Guttsche, C. Knapp, H. Scherer and R. Uzun, *Dalton Trans.*, 2009, 2687-2694.
- A. Avelar, F. S. Tham and C. A. Reed, *Angew. Chem. Int. Ed.*, 2009, **48**, 3491-3493.
- C. Bolli, J. Derendorf, M. Keßler, C. Knapp, H. Scherer, C. Schulz and J. Warneke, *Angew. Chem. Int. Ed.*, 2010, **49**, 3536-3538.
- I. Tiritiris and T. Schleid, *Z. Anorg. Allg. Chem.*, 2001, **627**, 2568-2570.
- M. A. Juhasz, G. R. Matheson, P. S. Chang, A. Rosenbaum and D. H. Juers, *Synth. React. Inorg., Met.-Org., Nano-Met. Chem.*, 2016, **46**, 583-588.
- J. W. Johnson and M. S. Whittingham, *J. Electrochem. Soc.*, 1980, **127**, 1653-1654.
- O. Tutusaus and R. Mohtadi, *ChemElectroChem*, 2015, **2**, 51-57.
- P. Kaszynski and A. G. Douglass, *J. Organomet. Chem.*, 1999, **581**, 28-38.
- B. Ringstrand, *Liquid Crystals Today*, 2013, **22**, 22-35.
- M. Kessler, C. Knapp, V. Sagawe, H. Scherer and R. Uzun, *Inorg. Chem.*, 2010, **49**, 5223-5230.
- W. Gu, M. R. Haneline, C. Douvris and O. V. Ozerov, *J. Am. Chem. Soc.*, 2009, **131**, 11203-11212.
- M. Wegener, F. Huber, C. Bolli, C. Jenne and S. F. Kirsch, *Chem. - Eur. J.*, 2015, **21**, 1328-1336.
- C. Knapp, *Comprehensive Inorganic Chemistry II*, Elsevier, 2013, 651-679.
- W. H. Sweet, *N Engl J Med*, 1951, **245**, 875-878.
- M. F. Hawthorne and A. Maderna, *Chem. Rev.*, 1999, **99**, 3421-3434.
- N. S. Hosmane, *Boron science: new technologies and applications*, CRC press, 2016.
- J. Warneke, G.-L. Hou, E. Aprà, C. Jenne, Z. Yang, Z. Qin, K. Kowalski, X.-B. Wang and S. S. Xantheas, *J. Am. Chem. Soc.*, 2017, **139**, 14749-14756.
- E. Aprà, J. Warneke, S. S. Xantheas and X.-B. Wang, *J. Chem. Phys.*, 2019, **150**, 164306.
- J. Warneke, C. Jenne, J. Bernarding, V. A. Azov and M. Plaumann, *Chem. Commun.*, 2016, **52**, 6300-6303.
- R. Challa, A. Ahuja, J. Ali and R. Khar, *AAPS PharmSciTech*, 2005, **6**, E329-E357.
- J. Zhang and P. X. Ma, *Adv. Drug Deliv. Rev.*, 2013, **65**, 1215-1233.
- J. Li and X. J. Loh, *Adv. Drug Deliv. Rev.*, 2008, **60**, 1000-1017.
- J. Taraszewska and J. Wójcik, *Supramol. Chem.*, 1993, **2**, 337-343.
- J. L. Pursell and C. J. Pursell, *J. Phys. Chem. A*, 2016, **120**, 2144-2149.

28. Y. Wu, R. Shi, Y.-L. Wu, J. M. Holcroft, Z. Liu, M. Frasconi, M. R. Wasielewski, H. Li and J. F. Stoddart, *J. Am. Chem. Soc.*, 2015, **137**, 4111-4118.
29. S. M. Eyrilmez, E. Bernhardt, J. Z. Dávalos, M. Lepšík, P. Hobza, K. I. Assaf, W. M. Nau, J. Holub, J. M. Oliva-Enrich and J. Fanfrlík, *Phys. Chem. Chem. Phys.*, 2017, **19**, 11748-11752.
30. K. I. Assaf, M. S. Ural, F. Pan, T. Georgiev, S. Simova, K. Rissanen, D. Gabel and W. M. Nau, *Angew. Chem. Int. Ed.*, 2015, **54**, 6852-6856.
31. K. I. Assaf and W. M. Nau, *Angew. Chem. Int. Ed.*, 2018, **57**, 13968-13981.
32. X.-B. Wang and L.-S. Wang, *Rev. Sci. Instrum.*, 2008, **79**, 073108.
33. T. Lu, *Molclus Program* (Beijing Kein Research Center for Natural Science, 2016), <http://www.keinrc.com/research/molclus.html>.
34. M. Korth, *J. Chem. Theory Comput.*, 2010, **6**, 3808-3816.
35. J. J. Stewart, *J. Mol. Model.*, 2007, **13**, 1173-1213.
36. C. Lee, W. Yang and R. G. Parr, *Phys. Rev. B*, 1988, **37**, 785.
37. A. D. Becke, *J. Chem. Phys.*, 1993, **98**, 5648-5652.
38. S. Grimme, S. Ehrlich and L. Goerigk, *J. Comput. Chem.*, 2011, **32**, 1456-1465.
39. P. C. Hariharan and J. A. Pople, *Theoret. Chim. Acta*, 1973, **28**, 213-222.
40. M. M. Francl, W. J. Pietro, W. J. Hehre, J. S. Binkley, M. S. Gordon, D. J. DeFrees and J. A. Pople, *J. Chem. Phys.*, 1982, **77**, 3654-3665.
41. Y. Zhao and D. G. Truhlar, *Theor. Chem. Acc.*, 2008, **120**, 215-241.
42. S. Grimme, J. Antony, S. Ehrlich and H. Krieg, *J. Chem. Phys.*, 2010, **132**, 154104.
43. M. J. Frisch, J. A. Pople and J. S. Binkley, *J. Chem. Phys.*, 1984, **80**, 3265-3269.
44. A. D. McLean and G. S. Chandler, *J. Chem. Phys.*, 1980, **72**, 5639-5648.
45. R. Krishnan, J. S. Binkley, R. Seeger and J. A. Pople, *J. Chem. Phys.*, 1980, **72**, 650-654.
46. M. J. Frisch, J. A. Pople and J. S. Binkley, *J. Chem. Phys.*, 1984, **80**, 3265-3269.
47. T. Clark, J. Chandrasekhar, G. W. Spitznagel and P. V. R. Schleyer, *J. Comput. Chem.*, 1983, **4**, 294-301.
48. C. Adamo and V. Barone, *J. Chem. Phys.*, 1999, **110**, 6158-6170.
49. S. F. Boys and F. d. Bernardi, *Mol. Phys.*, 1970, **19**, 553-566.
50. C. Lefebvre, G. Rubez, H. Khartabil, J.-C. Boisson, J. Contreras-García and E. Hénon, *Phys. Chem. Chem. Phys.*, 2017, **19**, 17928-17936.
51. E. R. Johnson, S. Keinan, P. Mori-Sánchez, J. Contreras-García, A. J. Cohen and W. Yang, *J. Am. Chem. Soc.*, 2010, **132**, 6498-6506.
52. T. Lu and F. Chen, *J. Comput. Chem.*, 2012, **33**, 580-592.
53. B. Jeziorski, R. Moszynski and K. Szalewicz, *Chem. Rev.*, 1994, **94**, 1887-1930.
54. E. G. Hohenstein and C. D. Sherrill, *J. Chem. Phys.*, 2010, **132**, 184111.
55. E. Papajak, J. Zheng, X. Xu, H. R. Leverentz and D. G. Truhlar, *J. Chem. Theory Comput.*, 2011, **7**, 3027-3034.
56. J. M. Turney, A. C. Simmonett, R. M. Parrish, E. G. Hohenstein, F. a. Evangelista, J. T. Fermann, B. J. Mintz, L. a. Burns, J. J. Wilke; M. L. Abrams, N. J. Russ, M. L. Leininger, C. L. Janssen, E. T. Seidl, W. D. Allen, H. F. Schaefer, R. a. King, E. F. Valeev, C. D. Sherrill and T. D. Crawford, *WIREs Comput. Mol. Sci.* 2012, **2**, 556-565.
57. W. D. Cornell, P. Cieplak, C. I. Bayly, I. R. Gould, K. M. Merz, D. M. Ferguson, D. C. Spellmeyer, T. Fox, J. W. Caldwell and P. A. Kollman, *J. Am. Chem. Soc.*, 1995, **117**, 5179-5197.
58. A. K. Rappé, C. J. Casewit, K. Colwell, W. A. Goddard III and W. M. Skiff, *J. Am. Chem. Soc.*, 1992, **114**, 10024-10035.
59. M. Frisch, G. Trucks, H. Schlegel, G. Scuseria, M. Robb, J. Cheeseman, G. Scalmani, V. Barone, G. Petersson, H. Nakatsuji and *et al.* *Gaussian 16 Rev. A.03; Gaussian Inc., Wallingford, CT, 2016.*
60. Z. Li, Z. Hu, Y. Jiang, Q. Yuan, H. Sun, X.-B. Wang and Z. Sun, *J. Chem. Phys.*, 2019, **150**, 244305.
61. L. Goerigk and S. Grimme, *Phys. Chem. Chem. Phys.*, 2011, **13**, 6670-6688.
62. X.-B. Wang, *J. Phys. Chem. A*, 2017, **121**, 1389-1401.
63. J. Zhang, B. Zhou, Z.-R. Sun and X.-B. Wang, *Phys. Chem. Chem. Phys.*, 2015, **17**, 3131-3141.
64. D. J. Tozer and N. C. Handy, *J. Chem. Phys.*, 1998, **109**, 10180-10189.
65. W. C. Geng, S. Jia, Z. Zheng, Z. Li, D. Ding and D. S. Guo, *Angew. Chem.*, 2019, **131**, 2399-2403.
66. C. Lefebvre, H. Khartabil, J. C. Boisson, J. Contreras - García, J. P. Piquemal and E. Hénon, *ChemPhysChem*, 2018, **19**, 724-735.
67. W. T. Klooster, T. F. Koetzle, P. E. Siegbahn, T. B. Richardson and R. H. Crabtree, *J. Am. Chem. Soc.*, 1999, **121**, 6337-6343.
68. Y. S. Chua, H. Wu, W. Zhou, T. J. Udovic, G. Wu, Z. Xiong, M. W. Wong and P. Chen, *Inorg. Chem.*, 2012, **51**, 1599-1603.
69. R. H. Crabtree, P. E. M. Siegbahn, O. Eisenstein, A. L. Rheingold and T. F. Koetzle, *Acc. Chem. Res.*, 1996, **29**, 348-354.
70. R. Custelcean and J. E. Jackson, *Chem. Rev.*, 2001, **101**, 1963-1980.
71. M. Brown and R. Heseltine, *Chem. Commun. (London)*, 1968, 1551-1552.
72. J.-P. Xue, W.-J. Wu, Q.-S. Li, Z.-S. Yao and J. Tao, *Inorg. Chem.*, 2019, **58**, 15705-15709.

